

# We are IntechOpen, the world's leading publisher of Open Access books Built by scientists, for scientists

6,900

Open access books available

185,000

International authors and editors

200M

Downloads

Our authors are among the

154

Countries delivered to

TOP 1%

most cited scientists

12.2%

Contributors from top 500 universities



WEB OF SCIENCE™

Selection of our books indexed in the Book Citation Index  
in Web of Science™ Core Collection (BKCI)

Interested in publishing with us?  
Contact [book.department@intechopen.com](mailto:book.department@intechopen.com)

Numbers displayed above are based on latest data collected.  
For more information visit [www.intechopen.com](http://www.intechopen.com)



# Image Fusion Based Enhancement of Nondestructive Evaluation Systems

Ibrahim Elshafiey, Ayed Algarni and Majeed A. Alkanhal  
*King Saud University  
 Saudi Arabia*

## 1. Introduction

Advantages and limitations associated with each nondestructive evaluation (NDE) modality raises a tradeoff in which no single modality can be identified for a particular application. Techniques are presented here that can be used to enhance inspection process based on multi-spectral, multi-temporal, and multi-resolution image fusion. The necessary elements for building an intelligent NDE system based on image fusion are introduced. An application is presented considering the fusion of optical and eddy current images. Developed image evaluation measures (quality metrics) are adopted to cross the gap between subjective and objective evaluation, which is essential to automate NDE systems in industrial environments.

## 2. Multimodal NDE

NDE methods involve the application of a suitable form of energy to the specimen under test. Wide variety of testing methods exists, where each method has certain properties and offers advantages, while having its drawbacks. The basic categories of NDE methods are: visual and optical testing (VT), radiography (RT) magnetic particle testing (MT), ultrasonic testing (UT), penetrant testing (PT), leak testing (LT) acoustic emission testing (AE), and electromagnetic testing (ET). Electromagnetic testing modalities are attractive for NDE applications due to the maturity and robustness of use of these techniques. The adopted ranges of the operating frequency cover almost the entire electromagnetic spectrum. Techniques employing the static operation, such as the magnetic flux leakage, and the quasi-static frequency range such as eddy current methods are commonly used more in industry than higher frequency (Lord, 1983). However, attention is being made to the higher end of the spectrum. Examples include application of microwave imaging techniques in inspecting civil structures (Cantor, 1984). Thermal waves are being used in characterization coating adhesion (Jaarinen et al., 1989), and optical methods are implemented in evaluating concrete and composite materials (Ansari, 1992). Ionizing radiation frequency ranges such as x-ray techniques are famous in tomographical reconstruction of defects and in assessing residual stresses. Among the ET modalities, the EC techniques get considerable attention, since they do not require hazard precautions as in the case of ionization radiation, in addition to the fact that they do not lack time information as for the static range.

NDE systems that are capable of extracting and fusing complementary segments of information from collected NDE data offer additional insight relative to the conventional systems. Fusion techniques are expected to play a major role in the next-generation NDE systems (Algarni et al., 2009). Fusion can make use of data collected from various NDE modalities, or even from the same technique operated at different points of time or using various parameter values (Elshafiey et al., 2008).

3. NDE signal fusion

NDE data fusion can be traced back to early 90s (Gros & Takahashi, 1998). Data fusion algorithms in NDE can be broadly classified as phenomenological or non-phenomenological. Phenomenological algorithms utilize knowledge of the underlying physical processes as a basis for deriving the procedure for fusing data. However, such methods are likely to be difficult to derive and cumbersome to implement (Simone & Morabito, 2001). Non-phenomenological approaches, in contrast, tend to ignore the physical process and attempt to fuse information based on the statistics associated with individual segments of data. The later methods can be classified into three different categories: pixel level, feature level and symbol level fusion, according to the stage at which fusion takes place as illustrated in Fig. 1.

Pixel based fusion requires accurate registration of the images to each other. Feature level fusion operate on mapped versions of original images. Decision (symbol) level fusion represents a method that implements value-added data obtained from processing the input images individually for information extraction, before applying decision rules.

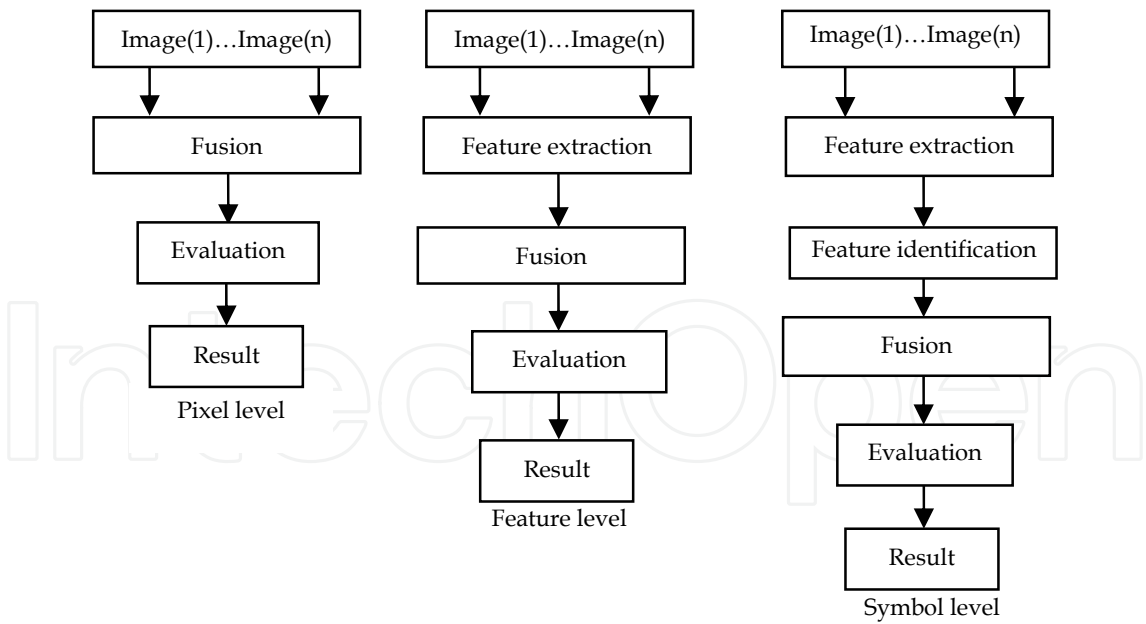


Fig. 1. NDE image fusion categories

4. NDE fusion algorithms

Various algorithms have been developed for NDE data fusion to improve the reliability and the performance of testing. The most widely applied are summarized next.

#### 4.1 Linear minimum mean square error (LMMSE)

This optimal approach uses a LMMSE filter to fuse multiple images, which was proposed in (Yim, 1995). The architecture of the fusion algorithm is given in Fig. 2. From system point of view,  $s(u,v)$  is the input signal to the system with the degradation transfer function  $H_i(u,v)$  associated with  $i^{\text{th}}$  stage,  $1 \leq i \leq N$ . From NDE point of view,  $s(u,v)$  is the perfect response of the original signal in the inspection process. The measurement system acquires signal  $x_i(u,v)$  with additive noise  $n_i(u,v)$ . Applying a controller filter  $G_i(u,v)$ , the output signal  $\tilde{s}(u,v)$  is controlled to have a minimum mean square error with the input signal.  $G_i(u,v)$  can be constructed from the spectra of the acquired images as follows:

$$G_j(u,v) = \frac{\sqrt{S_s(u,v)S_{xj}(u,v)}}{\sum_{i=1}^N S_{xi}(u,v)} \quad 1 \leq j \leq N \quad (1)$$

$G_j(u,v)$  is the  $j^{\text{th}}$  filter,  $S_s(u,v)$  is the Laplace transform of the original signal  $s(u,v)$ , and  $S_{xj}(u,v)$  is the Laplace transform of the  $j^{\text{th}}$  acquired image.

The spectrum of the original signal is approximated as (Yim, 1995)

$$G_j(u,v) = K \frac{\sqrt{S_{xj}(u,v)}}{\sum_{i=1}^N S_{xi}(u,v)} \quad 1 \leq j \leq N \quad (2)$$

Where,  $K$  is estimated spectrum which can be estimated by using the coefficients of Fourier decomposition of the signal.

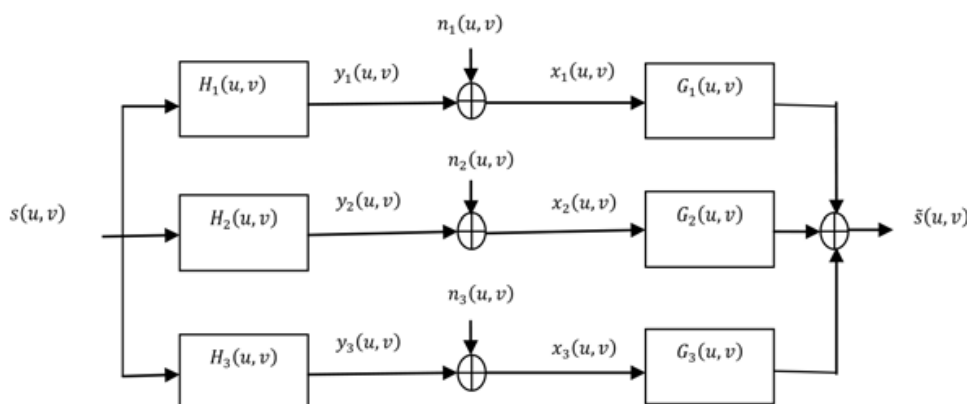


Fig. 2. Model for linear signal fusion

#### 4.2 Neural networks (NN) fusion

An attempt to fuse eddy current and ultrasonic images, and the other to fuse multi-frequency eddy current images are proposed as in (Yim et al., 1996), and (Udpa, 2001). Networks types implemented in fusion algorithms include multilayer perceptron (MLP) as well as radial basis function (RBF). The MLP network consists of a set of simple nonlinear processing elements that are arranged in layers and connected via adjustable weights. The network is usually trained using an appropriate algorithm such as back-propagation algorithm to estimate the interconnection weights. In RBF networks, the output nodal values are a linear combination of the basis functions that are calculated by the hidden layer nodes. A variety of basis functions can be employed, and Gaussian function is the most common

type. The MLP-based algorithm is sensitive to the choice of data used during the training phase. The RBF-based system fuses the image inputs smoothly reflecting information from input images.

### 4.3 Multi-resolution analysis (MRA) fusion

In this approach, the input NDE image is decomposed into a set of spatial frequency band pass sub-images. The sub-band images are computed by convolving and sub-sampling operations, as presented in (Gros et al., 2000); (Liu et al., 1999) and (Matuszewski et al., 2000). The multi-resolution analysis fusion techniques include the image pyramid approaches and wavelet based approaches. Different implementations of multi-resolution fusion are presented in Table 1, and are discussed next.

#### 4.3.1 Gaussian and Laplacian pyramid

Image pyramid consists of a set of low pass (Gaussian pyramid) or band pass (Laplacian pyramid) copies of an image, representing pattern information of a different scale. Burt and Adelson proposed Laplacian pyramid in 1983 (Gonzalez & Woods, 2007). The pyramid can be used for image compression and processing. Two operation involved are the EXPAND and REDUCE. The relation between two sub-images at level  $l$  and  $l-1$  is:

$$G_l = REDUCE(G_{l-1}) \quad (3)$$

EXPAND is defined as the reverse of REDUCE function and its effect is to expand an  $(M + 1)$  by  $(N + 1)$  array into a  $(2M + 1)$  by  $(2N + 1)$  array.

#### 4.3.2 Ratio of low pass pyramid

This is also based on the Gaussian pyramid, and the ratio of low pass pyramid is defined is introduced in (Toet, 1992) as:

$$R_l = \frac{G_l}{EXPAND(G_{l+1})} \text{ for } 0 \leq l \leq K \text{ \& } R_K = G_K \quad (4)$$

The perceptually important details are revealed by this kind of representation.

#### 4.3.3 Wavelet fusion

Multi-resolution analysis using wavelet transforms allows decomposing images into a set of new images with coarser and coarser spatial resolution (approximation images). The discrete approach of the wavelet transform mainly can be performed using two algorithms: discrete wavelet transform (DWT) also called decimated algorithm, and shift invariant discrete wavelet transform (SIWT), un-decimated discrete wavelet transform:

**Decimated Algorithm:** It is a fast DWT algorithm based on a multi resolution dyadic scheme that allows to decompose an image  $A^i$ , into an approximation image  $CA^{i+1}$  and three detail coefficient images,  $CV^{i+1}$ ,  $CH^{i+1}$ , and  $CD^{i+1}$ , where  $i$  is the level of the decomposition. If the original image  $A^i$  has  $C$  columns and  $R$  rows, the approximation and the wavelet coefficient images obtained applying this multi-resolution decomposition have  $C/2$  columns and  $R/2$  rows. The computation of the approximation and the detail coefficients is accomplished with a pyramidal scheme based on convolutions along rows

and columns with one-dimensional filters followed by a sub-sampling or decimation operation. When the multi-resolution wavelet decomposition process is inverted, the original image  $A^i$  can be reconstructed exactly from an approximation and detailed images, applying an up-sampling or oversampling process followed by filtering. To get an image fusion, wavelet decomposition is applied for input images, followed by integration of these decomposition coefficients to produce a composite representation. An inverse discrete wavelet transform is applied to get the fused image. The wavelet base fusion technique can reduce color distortion. Furthermore, the down sampling process may cause shift variation, which increases the distortion in the fused images.

**Un-decimated Algorithm:** This algorithm is based on the idea of no decimation. It is a redundant wavelet transform algorithm based on a multi-resolution dyadic scheme accomplished not with a pyramidal scheme but with a parallelepipedic scheme. The original image is decomposed as into four coefficients as in DWT but without decimation. All the approximation and wavelet coefficient images obtained by applying this algorithm have the same number of columns and rows as the original image thus such decomposition is highly redundant. Based on (Li et al., 2002) the performance of the SIWT based algorithm outperforms the DWT based fusion algorithms.

MRA Method	Algorithm	Rule of fusion
Gaussian and Laplacian Pyramid	Sequence of images in which each member of the sequence is a low pass filtered or band pass version of its predecessor	-Coefficient selection based on maximum absolute value. -Coefficient selection or average based on salience and match measure.
Ratio of Low Pass Pyramid	Every level the image is the ratio of two successive levels of the Gaussian pyramid	Coefficient selection based on maximum absolute contrast.
Discrete Wavelet Transform (DWT)	Images are decomposed via wavelet transform, after applying the rule of fusion, then inverse discrete wavelet transform is found	Selection based on choosing the maximum absolute values, or an area based maximum energy
Shift Invariant Discrete Wavelet Transform (SIDWT)	SIDWT is obtained using à trous algorithm so the process of fusion is independent of the location of an object in the image	

Table 1. MRA based image fusion algorithms

Wavelet Image Fusion Rules

Several rules can be used for selecting the wavelet packet coefficients for image fusion. The most frequently used fusion rules are:

- **Maximum frequency rule.** The coefficients with the highest absolute value indicating salient features are selected.

- **Weighted average rule.** It generates a coefficient via a weighted average of the two images' coefficients, where the weighting coefficients are based on the correlation between the two images.
- **Standard deviation rule.** It calculates an activity or energy measure associated with a pixel. A decision map is created, which indicates the source image from which the coefficient has to be selected.
- **Window based verification rule.** It creates a binary decision map to choose between each pair of coefficients using a majority filter.

## 5. Implementation examples of NDE signal fusion

Implementation examples of fusion methods in some of the NDE applications are presented next, along with by a brief summary of related literature listed in Table 2.

### 5.1 Fusion of eddy current signals

A fusion algorithm is proposed using the data from both real and imaginary image components using artificial cracks around rivet holes in an aluminum specimen in (Mina et al., 1997). The operation is implemented in the transform domain with the discrete Fourier transform. The fusion process is based on the spectrum of the acquired signal, where the linear minimum mean square error (LMMSE) approach was adopted to fuse the images using a weighting scheme. Multi-frequency eddy current testing (MF-ET) is implemented in (Mina et al., 1996) to enhance SNR. Two ET scan images obtained at 6 and 20 KHz, with radial basis function (RBF) neural networks. A relatively clear display of subsurface flows is achieved after the fusion process. Pixel level fusion technique using a multi-resolution image pyramid was proposed in (Liu et al., 1999). Signals from two different ET systems in weld inspection, are fused using the Dempster-Shafer (DS) combination rule in (Gros et al., 1995), achieving accurate estimation of crack size.

### 5.2 Fusion of ultrasonic signals

Amplitude, frequency, or time of flight of the echo signals provides information about the nature and position of flaws. Ultrasonic testing produces high resolution measurements but the signal is affected by the surface roughness of the specimen and grain structure of metals. Ultrasonic image is fused with eddy current images using the AND operation in (Song & Udpa, 1996) in order to take advantage of both methods. Experiments were carried out on an aluminum plate where a simulated defect was present. The boundary of the defect was extracted from the UT image, whereas the depth information could be characterized from an ET image. Another way to fuse UT and ET data is the use of RBF NNs or multilayer perceptron (MLP). The experiments were carried out in (Simone & Morabito, 2001) to fuse eddy current and ultrasonic images showed that the fusion operation improves the process of defect classification.

### 5.3 Fusion of other NDE modalities

Infrared (IR) thermographic testing and ET C-scan is fused using wavelet-based methods, where an impacted carbon fiber reinforced plastic composite panel is used in (Gros, Liu, Tsukada, & Hanaski, 2000) (Gros et al., 2000) and (Liu et al., 1999). Application of multiple inspection techniques for NDE fusion is presented in increasing (Tian et al., 2005); (Volponi et al., 2004) and (Kaftandjian et al., 2005).

## 6. Image visualization of NDE signals

Data visualization is an effective and intuitive method for understanding the results of inspection. An effective data visualization stage helps improve the evaluation, especially in quantitative evaluation of types, locations, sizes and shapes of the defects. On the other hand, imaging reduces the necessity for highly qualified inspector for interpretation of the results. Imaging also gives the ability to use the advanced image processing techniques for further improvements as image. Casting NDE data on image format allows also application of image fusion techniques. Image registration however is essential in this process to allow robust fusion results. Image registration is discussed next followed by the techniques which are used to present eddy current data, normally presented as one-dimensional signal form in two-dimensional c-scan image format.

### 6.1 Image registration

Registration is the process, which determines the best match of two or more images acquired at the same or various times by different or identical sensors. One image is used as the reference image, and all the other images are matched relative to this reference data. Match can be performed at the one-dimensional level, the two-dimensional level and the three-dimensional level. The majority of the registration methods consist of the following four steps (Zitova & Flusser, 2003):

**Selection of feature points.** Salient and distinctive objects (closed-boundary regions, edges, contours, line intersections, corners, etc.) are manually or, preferably, automatically detected. These points are called control points.

**Feature matching.** In this step, the correspondence between the features detected in the input image and those detected in the reference image is established.

**Transform model estimation.** The type and parameters of the so-called mapping functions, aligning the input image with the reference image, are estimated. The parameters of the mapping functions are computed by means of the established feature correspondence.

**Image re-sampling and transformation.** The input image is transformed by means of the mapping functions. Image values in non-integer coordinates are computed by the appropriate interpolation technique.

### 6.2 Eddy current imaging

Various techniques have been developed to present eddy current inspection data in the form of C-scan images. Probe impedance values acquired in two dimensional surface scans provide a set of ranges (Udpa & Elshafiey, 2001). Magnetic flux maps could also be presented in image format using techniques such as magneto-optic eddy current technology (Lee & Song, 2005) or giant magneto-resistive sensors GMR field scanning (Chalastaras et al., 2004).

### 6.3 Pulsed eddy current imaging

Pulsed eddy current sensing is an emerging technique that has been particularly developed for subsurface flow. These techniques can work at some distance below the surface (up to 100 mm in aluminum) (Tian et al., 2005). In PEC techniques the probe's excitation coil is excited with a repetitive broadband pulse, usually a rectangular wave. The resulting transient current through the coil induces transient eddy currents in the test object, which are associated with highly attenuated magnetic pulses propagating through the material.

Reference	Fusion Technique	Modality
(Tai & Pan, 2008)	Physical interaction / Human fusion	EC / photo inductive imaging
(Liu, Abbas, & Nezh, 2006)	Dempester-Shafer	EC / PEC
(Kaftandjian et al., 2005)	Evidence Theory / Fuzzy logic	X-Ray / Ultrasonic
(Chady et al., 2005)	Barkhausen noise method	EC / Flux leakage
(Djafari, July, 2002)	Bayesian	X-ray / Geometrical data
(Francois & Kaftandjian, 2003)	Dempester-Shafer	X-ray/ Ultrasonic
(Simone & Morabito, 2001)	Feed-forward Neural Networks (NN)	EC/Ultrasonic
(Udpa, 2001)	NN	EC/Ultrasonic
(Matuszewski et al. 2000)	Wavelet	Ultrasonic / radiographic
(Brassard et al., 2000)	Image subtraction	Edge of light / PEC
(Liu et al., 1999)	Multiresolution Analysis (MRA )	Multi-frequency EC
(Mina et al., 1996)	Image Pyramid	Multi-frequency EC
(Mina et al., 1997)	DFT/LMMSE	Real/imaginary of Z
(Song & Udpa, 1996)	Image Pyramid	Ultrasonic/EC
(Yim et al., 1996)	NN	Multi-frequency EC
(Yim et al., 1995)	NN	Ultrasonic/EC
(Yim, 1995)	LMMSE	Ultrasonic/EC
(Liu et al., 1999)	MRA	Multi-frequency EC

Table 2. Fusion algorithms applied to NDE applications

The probe provides a series of voltage-time data pairs as the induced field decays, and since the produced pulses consist of a broad frequency spectrum, the reflected signal contains important depth information, physically, the field is broadened and delayed as it travels deeper into the highly dispersive material. Flaws or other anomalies close to the surface affect the eddy current response earlier than deeper flaws. Peak values, time to maximum values, and time to minimum values have been used for flaw detection and identification. Features are selected based on knowledge about the possible crack that might be most probably happened. In surface cracks the amplitude feature gives better resolution, while the time feature gives more information about the subsurface cracks.

## 7. Fusion performance evaluation

In many applications, a human observer is the end user of the fused image. Therefore, the human perception and interpretation of the fused image is very important. Consequently, one way to assess the fused images is to use subjective tests. Although the subjective tests are typically accurate whenever performed correctly, they are inconvenient, expensive, and time consuming. Hence, an objective performance measure that can accurately predict human perception would be a valuable complementary method. However, it is difficult to find a good, easy to calculate, objective evaluation criterion which matches favorably with visual inspection and is suitable for a variety of different application requirements. In the literature, there are two broad classes of objective performance measures. One class requires a reference image, while the other does not (Wang et al., 2004).

### 7.1 Evaluation measures requiring a reference image

For certain applications, it is possible to generate an ideal fused image, which is then used as a reference to compare with the experimental fused results. The five quality metrics used for these comparisons are given next, where  $R$  denotes the reference image,  $F$  denotes the fused image,  $(i, j)$  denotes a given pixel,  $L$  denotes the number of gray levels, and  $N \times M$  is the size of the input image.

denotes the reference image,  $F$  denotes the fused image,  $(i, j)$  denotes a given pixel, and  $N \times M$  is the size of the image.

The root mean square error (RMSE)

$$RMSE = \sqrt{\frac{1}{NM} \sum_{i=1}^N \sum_{j=1}^M |R(i, j) - F(i, j)|^2} \quad (5)$$

The correlation (CORR)

$$CORR = \frac{2C_{R,F}}{C_R + C_F} \quad (6)$$

Where  $C_R = \sum_{i=1}^N \sum_{j=1}^M R(i, j)^2$ ,  $C_F = \sum_{i=1}^N \sum_{j=1}^M F(i, j)^2$  and  $C_{R,F} = \sum_{i=1}^N \sum_{j=1}^M R(i, j)F(i, j)$ .

The peak signal to noise ratio (PSNR)

$$PSNR = 10 \log_{10} \left( \frac{L^2}{\frac{1}{NM} \sum_{i=1}^N \sum_{j=1}^M |R(i,j) - F(i,j)|^2} \right) \quad (7)$$

The mutual information (MI)

$$MI = \sum_{i_1=1}^L \sum_{i_2=1}^L h_{R,F}(i_1, i_2) \log_2 \frac{h_{R,F}(i_1, i_2)}{h_R(i_1) h_F(i_2)} \quad (8)$$

where  $h_{R,F}$  denotes the normalized joint gray level histogram of images R and F while  $h_R, h_F$  are the normalized marginal histograms of the two images.

Structure information, structural similarity (SSIM)

This image quality assessment is proposed as (Wang et al., 2004) (Wang, Bovik, Sheikh, & Simoncelli, 2004)

$$SSIM = \frac{(2\mu_R\mu_F + C_1)(2\sigma_{RF} + C_2)}{(\mu_R^2 + \mu_F^2 + C_1)(\sigma_R^2 + \sigma_F^2 + C_2)} \quad (9)$$

where  $C_1$  is a constant that is included to avoid the instability when sum of mean of reference image R, and mean of fused image F is close to zero (i.e.  $\mu_R^2 + \mu_F^2 \approx 0$ ), and  $C_2$  is a constant that is included to avoid the instability when standard deviations is close to zero (i.e.  $\sigma_R^2 + \sigma_F^2 \approx 0$ )

The objective image quality measures: RMSE, PSNR, CORR and MI, are widely employed due to their simplicity. However, they have been found sometimes not correlate well with human evaluation when sensors of different types are considered (Blum & Liu, 2006) and the SSIM measure can be used.

## 7.2 Evaluation measures not requiring a reference image

It is generally difficult to access the ideal reference images. Several simple quantitative evaluation methods which do not require a reference image are listed below.

The standard deviation (SD)

$$\sigma = \sqrt{\sum_{i=0}^L (i - \bar{i})^2 h(i)} \quad (10)$$

where  $h$  is the normalized histogram of image and  $\sum_{i=0}^L ih(i)$ .

The entropy (H)

$$H = - \sum_{i=0}^L h(i) \log_2 h(i) \quad (11)$$

Petrovic quality index (QI)

An objective performance metric is proposed in (Petrovic, 2000), which measures the amount of information that is transferred from the input images into the fused image. Their

approach is based on the assumption that important visual information is related with edge information. A Sobel edge operator is applied to yield edge strength  $g(i,j)$  and orientation  $\alpha(i,j) \in [0, \pi]$  for each pixel of the image. The relative strength and orientation values,  $G^{AF}(i,j)$  and  $\Phi^{AF}(i,j)$ , of input image  $A$  with respect to fused image  $F$  are defined as:

$$G^{AF}(i,j) = \begin{cases} \frac{g_F(i,j)}{g_A(i,j)} & \text{if } g^F(i,j) > g^A(i,j) \\ \frac{g_A(i,j)}{g_F(i,j)} & \text{otherwise} \end{cases} \quad (12)$$

$$\Phi^{AF}(i,j) = 1 - \frac{|\alpha_A(i,j) - \alpha_F(i,j)|}{\pi / 2} \quad (13)$$

The edge preservation values  $Q^{AF}$  from input image  $A$  to fused result  $F$  is formed by the product of a sigmoid mapping function of the relative strength and orientation factors. Some constants as defined in (Petrovic, 2000)  $\kappa, \sigma$  and  $\Gamma$  determine the shape of the sigmoid mapping as

$$Q^{AF}(i,j) = \frac{\Gamma_g \Gamma_a}{\left(1 + \exp^{\kappa_g(G^{AF}(i,j) - \sigma_g)}\right) \left(1 + \exp^{\kappa_a(\Phi^{AF}(i,j) - \sigma_a)}\right)} \quad (14)$$

In equation (14), there are 6 parameters ( $\kappa_g, \sigma_g, \kappa_a, \sigma_a, \Gamma_g$ , and  $\Gamma_a$ ), where the first four parameters are determined via an optimization process that maximizes a correspondence measure between objective and subjective image fusion assessment results. Furthermore the constant  $\Gamma_g$  and  $\Gamma_a$  are selected such that for optimal values of  $\kappa_g, \sigma_g, \kappa_a, \sigma_a$  and  $G^{AF}, \Phi^{AF}$  equal to 1, the  $Q^{AF}$  will also be equal to 1 (Chen & Blum, 2005). The overall objective quality quantity measure  $QI^{AB/F}$  is obtained by weighting the normalized edge preservation values of both input images  $A$ , and  $B$  as:

$$QI^{AB/F} = \frac{\sum_{i=1}^N \sum_{j=1}^M Q^{AF}(i,j) w^A(i,j) + Q^{BF}(i,j) w^B(i,j)}{\sum_{i=1}^N \sum_{j=1}^M (w^A(i,j) + w^B(i,j))} \quad (15)$$

In general the weights  $w^A(i,j)$  and  $w^B(i,j)$  are a function of edge strength. The range of  $QI$  is between 0 and 1, where 0 indicates the complete loss of source information and 1 means the ideal fusion.

## 8. Proposed NDE fusion systems

Three proposed fusion systems based on IHS transformation, PCA, and multi-resolution wavelet decomposition (MWD) are presented next.

### 8.1 Intensity-hue-saturation (IHS) transform fusion

The IHS technique is a standard procedure in image fusion, and has fast computing capability for fusing images (Tania, 2008). The widespread use of the IHS transform to

merge remote sensing images is based on the ability to separate the spectral information of the RGB image into its two components ( $H$ ) and ( $S$ ), while isolating most of the spatial information in the ( $I$ ) component. The fusion steps can be summarized as:

**Register** three input images defined as  $R$ ,  $G$ , and  $B$  to the same size as the high resolution image defined as  $HR$ .

**Transform** the  $R$ ,  $G$ , and  $B$  false color image into the  $IHS$  component using one of the different transformations that have been developed to transfer a color image from the RGB space to the IHS space. The most common RGB- IHS conversion system is based on the following linear transformation (Gonzalez-Audicana et al., 2006), for each pixel  $p$ .

$$\begin{bmatrix} I^p \\ V_1^p \\ V_2^p \end{bmatrix} = \begin{bmatrix} \frac{1}{3} & \frac{1}{3} & \frac{1}{3} \\ -\frac{\sqrt{2}}{6} & -\frac{\sqrt{2}}{6} & -\frac{\sqrt{2}}{6} \\ \frac{1}{\sqrt{2}} & -\frac{1}{\sqrt{2}} & 0 \end{bmatrix} \begin{bmatrix} R^p \\ G^p \\ B^p \end{bmatrix} \quad (16)$$

$$H^p = \tan^{-1} \left( \frac{V_1^p}{V_2^p} \right) \quad (17)$$

$$S^p = \sqrt{(V_1^p)^2 + (V_2^p)^2} \quad (18)$$

**Modify** the  $HR$  image to accounts for differences related to acquisition techniques, this is usually performed by conventional histogram matching between the  $HR$  image and the intensity component  $I$  of the IHS representation (Nunez, 1999), i.e. after computing the histogram of both  $HR$  image and the intensity component  $I$  of the IHS representation, the histogram of the intensity component  $I$  is used as reference to which  $HR$  image histogram was matched, the new  $HR$  image defined as  $NHR$ .

**Replace** the intensity component  $I$  by the  $NHR$  image.

**Perform** the inverse transformation to obtain the merged  $R'G'B'$  fused image using the relations

$$\begin{bmatrix} R'^p \\ G'^p \\ B'^p \end{bmatrix} = \begin{bmatrix} 1 & \frac{-1}{\sqrt{2}} & \frac{1}{\sqrt{2}} \\ 1 & \frac{-1}{\sqrt{2}} & \frac{-1}{\sqrt{2}} \\ 1 & \sqrt{2} & 0 \end{bmatrix} \begin{bmatrix} NHR^p \\ V_1^p \\ V_2^p \end{bmatrix} \quad (19)$$

The generated fused image provides the full details of the  $HR$  image but introduces color distortion. This is because of the low correlation between the  $HR$  image and the intensity component  $I$ .

## 8.2 Principal component analysis PCA fusion

PCA provides a powerful tool for data analysis which is often used in signal and image processing (Gonzalez & Woods, 2007) as a technique for data compression, data dimension reduction, and data fusion. Original images constitute the input data, and the result of this

transformation is to obtain non-correlated new bands, called the principal components. PCA in signal processing can be described as a transform of a given set of  $n$  input vectors (variables) with the same length  $K$  formed in  $n$ -dimensional vector  $x = [x_1, x_2, \dots, x_n]^T$  into a vector  $y$  according to

$$y = P(x - m_x) \quad (20)$$

The vector  $m_x$  is the vector of mean values of all input variables defined by the relation

$$m_x = E\{x\} = \frac{1}{K} \sum_{k=1}^K x_k \quad (21)$$

Matrix  $P$  is determined by the covariance matrix  $C_x$ , where rows in  $P$  are formed from the eigenvectors  $e$  of  $C_x$  ordered according to corresponding eigenvalues in descending order. The evaluation of the  $C_x$  matrix is possible according to relation

$$C_x = E\{(x - m_x)(x - m_x)^T\} = \frac{1}{K} \sum_{k=1}^K x_k x_k^T - m_x m_x^T \quad (22)$$

For  $n$ -dimensional input vector  $x$ , the size of  $C_x$  is  $n \times n$ . The elements  $C_x(i,i)$  lying in its main diagonal are the variances of  $x$ , and the other values  $C_x(i,j)$  determine the covariance between input variables  $x_i, x_j$ . The rows of  $P$  are orthonormal so the inversion of PCA is possible.

Both IHS and PCA mergers are based on the same principle: to separate most of the spatial information of multispectral image from its spectral information by means of linear transforms. The IHS transform separates the spatial information of the multispectral image as the intensity ( $I$ ) component. In the same way, PCA separates the spatial information of the image into the first principal component PC1. PCA allows synthesizing the original bands creating new bands, the principal components, which pick up and reorganize most of the original information. In general, the first principal component PC1 collects the information that is common to all the bands used as input data in the PCA, i.e., the spatial information, while the spectral information that is specific to each band is picked up in the other principal components (Kwarteng & Chavez, 1989).

The proposed PCA method is similar to the described IHS method, with the main advantage that an arbitrary number of bands can be used as shown in Fig. 3. If more than three images to be fused using IHS, PCA is used as a first step. PC1 is replaced by the HR image, whose histogram has previously been matched with that of PC1. Finally, the inverse transformation is applied to the whole dataset formed by the modified HR image and the PC2, ... PCn.

### 8.3 Improved IHS based on multi-resolution wavelet decomposition (MWD) fusion

The IHS fusion method usually can integrate color and spatial features smoothly. If the correlation between the IHS intensity image and the HR image is high, the IHS fusion can well preserve the color information. However, the color distortion can be significant for low correlation values, between the intensity image and the HR image, especially when the input images and HR images originally from different sensors.

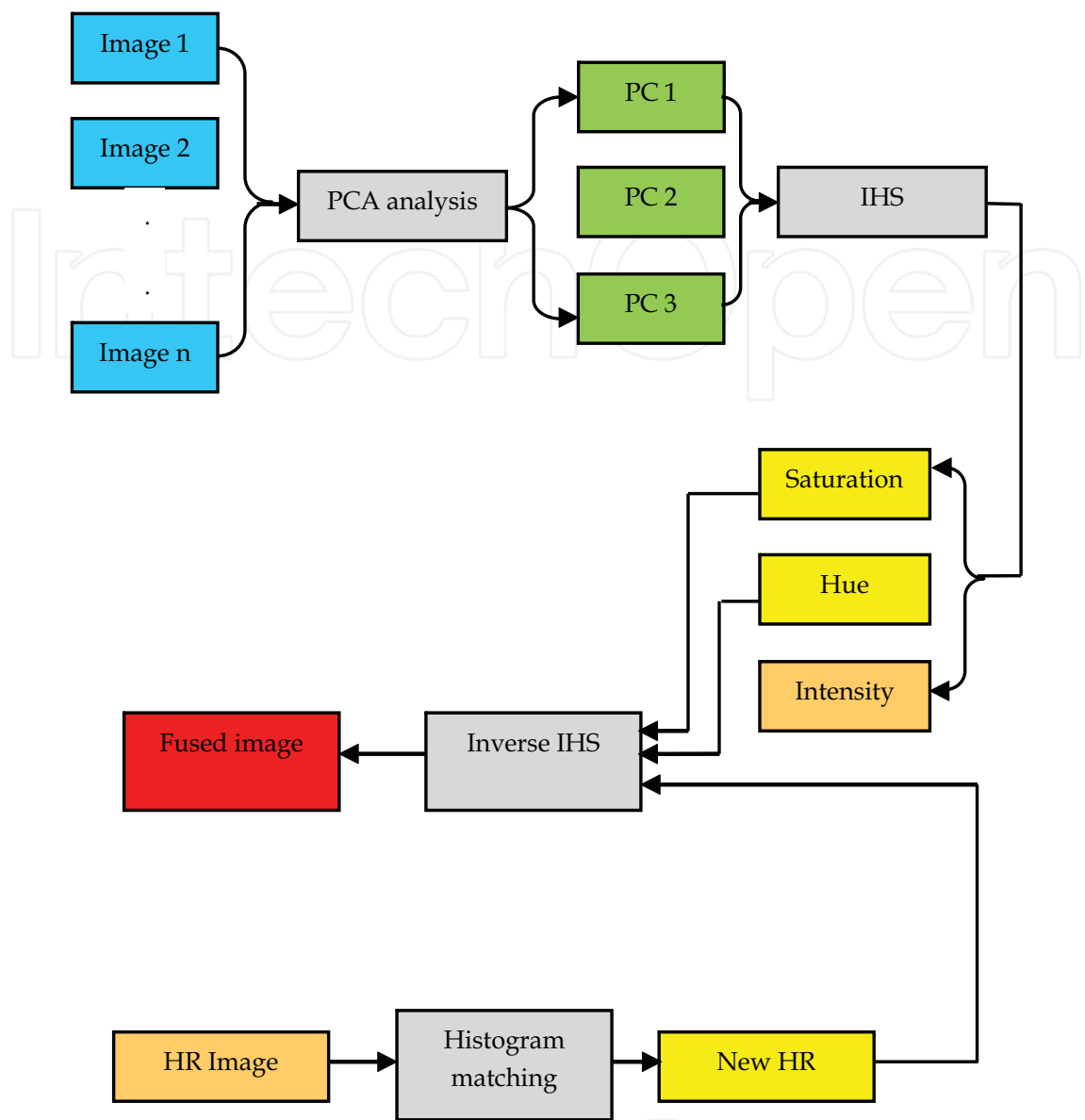


Fig. 3. Arbitrary number of inputs IHS fusion system

On the other hand, the discrete wavelet transform (DWT) image fusion can usually preserve color information better than other fusion methods, since the high-resolution spatial information from HR image is injected into all the three low-resolution multispectral bands. However, the spatial detail from HR image is often different from that of a multispectral band having the same spatial resolution. This difference may introduce some color distortion into the wavelet frame fusion results. To better utilize the advantages of the IHS and the DWT fusion techniques, and to overcome the shortcomings of the two techniques, an integrated IHS and wavelet frame fusion approach is proposed here as shown in Fig. 4. The shift invariant wavelet transform obtained using á trous (with holes) algorithm overcomes image artifacts (Wang et al., 2005) and (Fowler, 2005), the un-decimated multi-resolution wavelet decomposition (MWD) or shift invariant discrete wavelet transform (SIDWT) was used for the IHS fusion improvement.

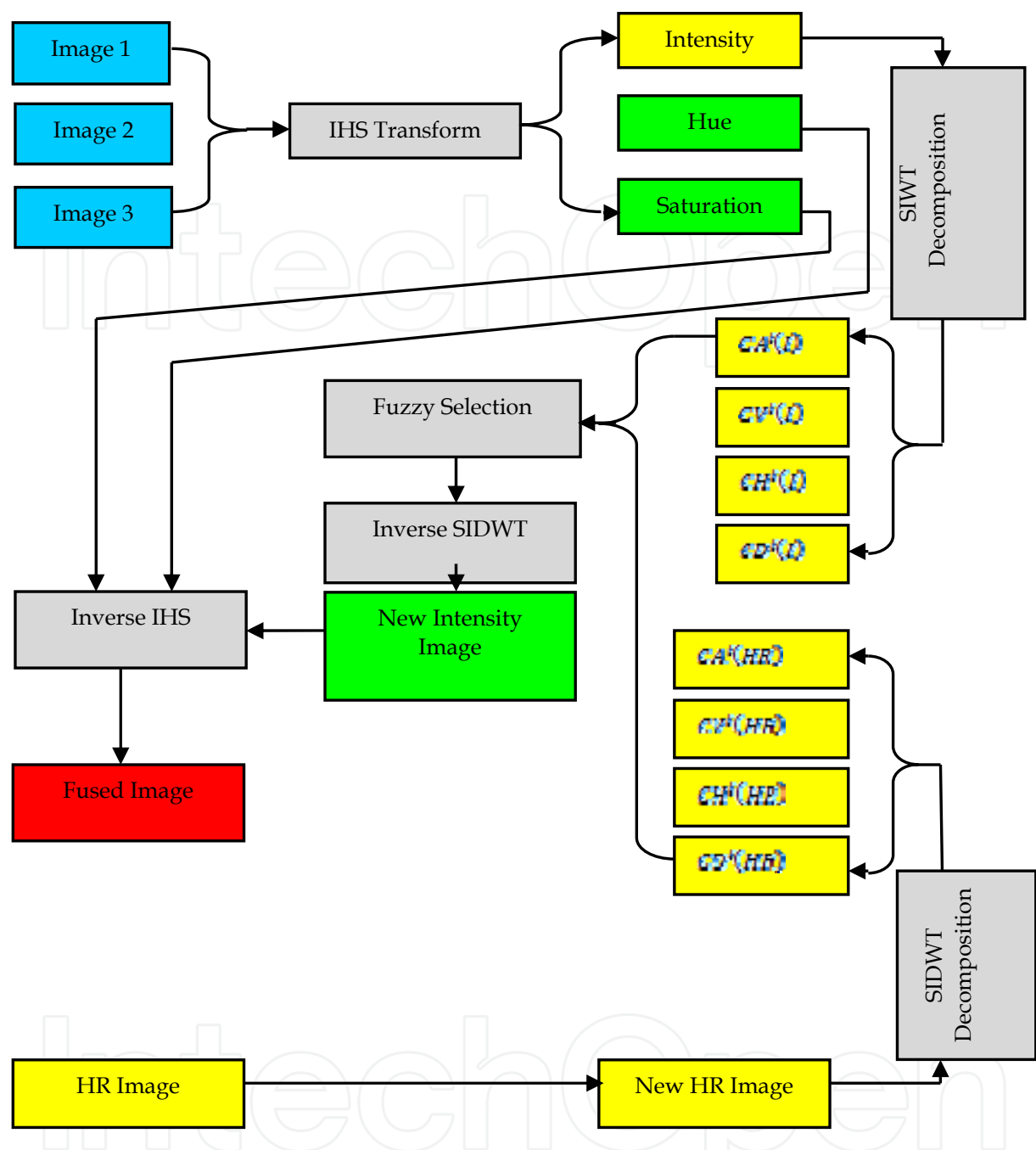


Fig. 4. Improved IHS fusion based on MWD

The steps of this approach are summarized as:

**Registration.** All images are first registered.

**IHS Transform.** the multispectral image is transformed into IHS components as illustrated before.

**Histogram match.** The histogram of the HR image and the intensity component  $I$  of the IHS color space are matched and a new HR image ( $NHR$ ) is obtained.

**SIDWT Decomposition:** Apply the un-decimated wavelet decomposition, to the intensity component  $I$  and to the corresponding histogram matched  $NHR$  image using the Daubechies four coefficient wavelet.

**Fuzzy selection:** after the decomposition has been made a selection based on the application needed should be made. For example one possible application is to fuse optical image that has information about the rivets and joints for example with inspection EC images, in this case the best selection would be to take the approximation of the optical image and the detail of the EC images. Another application is to replace high spatial resolution information with low spatial resolution of the fused images, in this case the detail of the *NHR* is selected.

**Inverse SIWT:** the shift invariant reconstruction transform applied to the selected wavelet coefficients to form the new intensity image.

**Inverse IHS transform:** The final fused image is generated by transforming the new intensity image together with the hue and saturation components back into RGB space.

8.4 NDE fusion results

The evaluation of the IHS proposed fusion with application to NDE were performed using simulation as well as experimental signals.

8.4.1 Simulation results

Fig. 5 presents ten images generated with 128x128 resolution, representing probe resistance values (images  $R_1$ - $R_5$ ) on the top row, and probe inductance values (images  $L_1$ - $L_5$ ) on the bottom row. Images  $R_1$  and  $L_1$  on the left side correspond to lowest frequency while  $R_5$  &  $L_5$  on the right side correspond to the highest frequency. First some of fusion results presented, before the presentation of a comparison of various fusion algorithms. Fig. 6 is based on IHS fusion with high frequency high-resolution PEC image generated at 256x256. Fig. 7 presents the first four principal components images computed from  $R_1$ - $R_5$  (the first row of Fig. 5). Examples of image fusion with shift invariant wavelet decomposition are presented in Fig. 8, where Daubechies wavelets of order 4 are used. Four images were selected to make the comparison of fusion algorithms that have been applied to the NDE technology with the proposed fusion algorithms. The selected simulation images presented in Fig. 9 were two frequency domain images, and two time domain images.

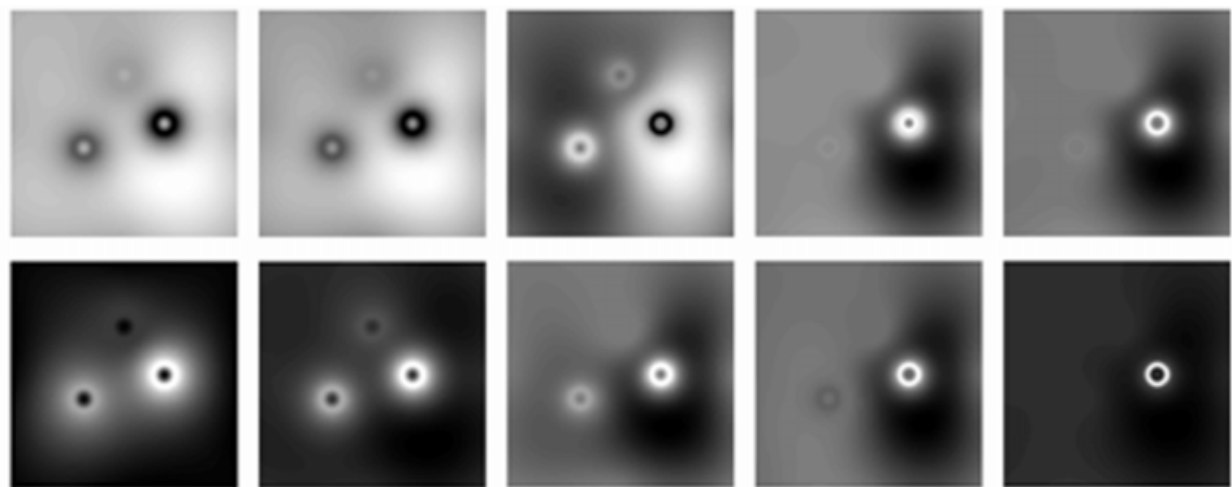


Fig. 5. Ten images representing probe resistance values  $R_1$ - $R_5$  (top row, left to right) and inductance values  $L_1$ - $L_5$  (bottom row, left to right) corresponding to five different frequency values: 100 Hz, 1 kHz, 10 kHz, 100 kHz, and 1M Hz

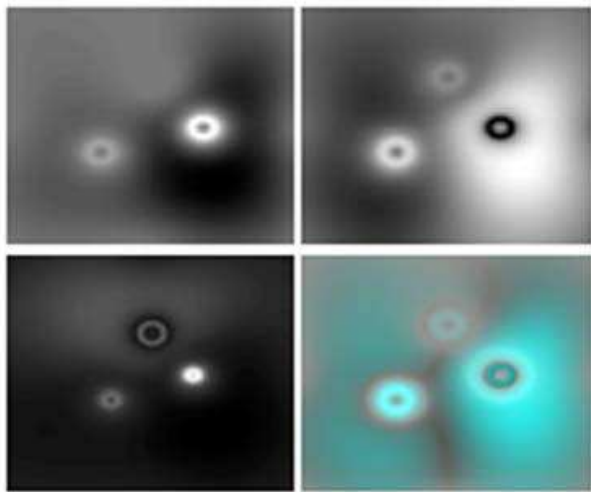


Fig. 6. Fusion obtained with IHS transformation. Top-left is  $L_3(10\text{ kHz})$  image, top-right is  $R_3(10\text{ kHz})$  image, down-left is PEC image and down-right is fused image

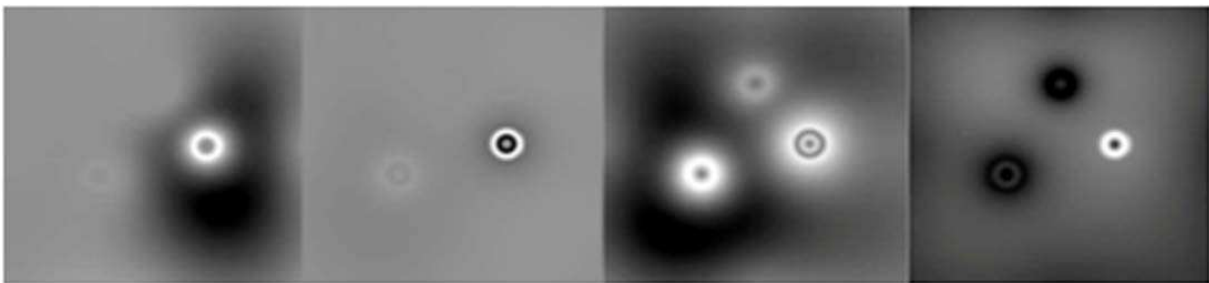


Fig. 7. The first four principal components images computed from  $R_1$ - $R_5$

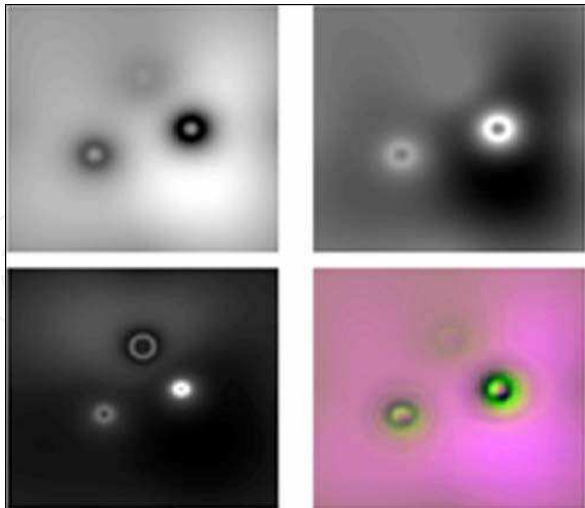


Fig. 8. Fusion obtained with wavelet decomposition, where the high spatial resolution image was taken as  $R_5$ . Top-left is  $R_2(1\text{ kHz})$  image, top-right is  $L_3(10\text{ kHz})$  image, down-left is PEC image and down-right is fused image

The proposed IHS based fusion algorithms, and the improved IHS based on MWD fusion termed as IHSW were compared with three fusion algorithms mostly presented in literature

with application to NDE i.e. the Laplacian pyramid (LAP), the discrete wavelet transform (DWT), and the shift invariant discrete wavelet transform (SIDWT). The maximum frequency rule was used which selects the coefficients with the highest absolute value for LAP, DWT, and SIDWT fusion methods.

Fig. 10 presents the fusion results of the compared fusion algorithms where the input images for all were shown in Fig. 9. Table 3 shows the estimated quality measure for these fused images. Notice that the standard deviation (SD) and the entropy (H) illustrated that the IHS based methods are better in performance, while .IHS based methods are not. There are six parameters in the QI performance measure that are determined via optimization process to maximize the correspondence measure between objective and subjective image fusion assessment. It is not thus a reliable performance measure for general application. Investigating these quality measure revealed that, a small change in these constant highly affect the performance.

Fusion method	Standard deviation (SD)	Entropy (H)	quality index (QI)
Laplacian pyramid (LAP)	30.1900	6.8695	0.7565
Discrete wavelet transform (DWT)	35.1318	6.8822	0.8077
Shift invariant discrete wavelet transform (SIDWT)	27.7046	6.7731	0.7588
Intensity hue saturation (IHS)	45.8145	7.1791	0.6008
Intensity hue saturation with wavelet (IHSW)	33.3772	7.3190	0.5484

Table 3. Comparison of the quality measures for the fused images shown in Fig. 10

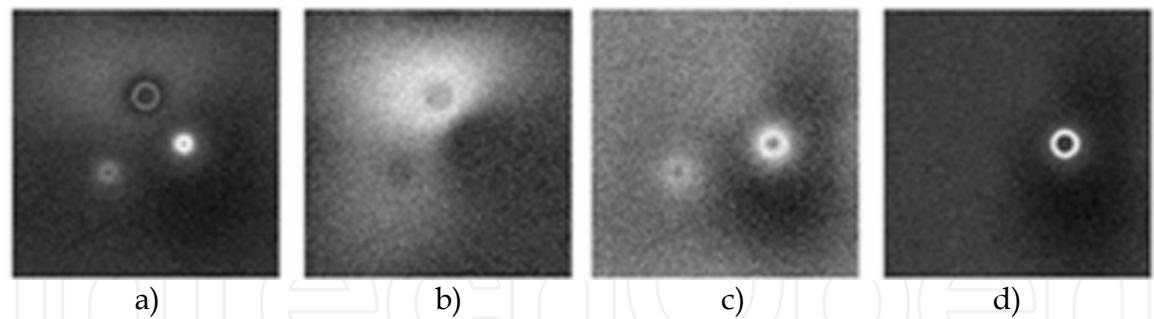


Fig. 9. Images used to evaluate the fusion algorithms, (a) maximum amplitude feature PEC image, (b) time to maximum PEC image, (c) probe-L image at 10 kHz, (d) probe-L at 1MHz as a HR

With the Gaussian noise added to the input images according to a predefined signal to noise ratio SNR, the performance of the fusion methods were compared with standard deviation SD, and entropy H, the results plotted in Fig. 11. It is clear from the results that the IHS based methods perform better. Also it is noticed out that the SD of the IHS based methods increases with the increase of SNR of input images. Entropy is used to measure the amount of uncertainty or information of an image, but it is sensitive to noise (Naidu & Raol, 2008). The dynamic range of SD and H are very small when the SNR exceed 20 dB which is typically the acceptable image SNR. Subjectively, IHS based fusion methods ranked higher than the other fusion methods.

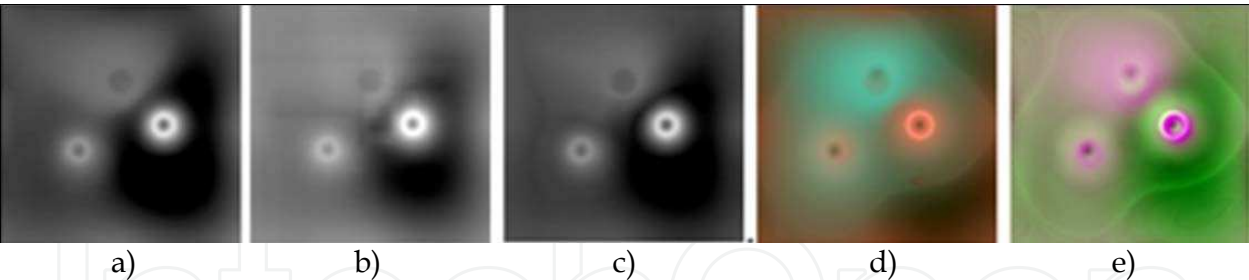


Fig. 10. Fusion results of the images shown in Fig. 7 using LAP (a), DWT (b), SIDWT (c), IHS (d), IHSW (e) techniques

8.4.2 Experimental eddy current images

Experimental EC images produced employing EC measurement device measurement system (Rohmann B300) (Rohmann Documentation), connected to a scanning system, based on six degree of freedom robot arm manufactured by Staubli (Staubli Documentation) which can gives a resolution of 0.1. The main parts of the system are shown in Fig. 12. The output of the EC measurement system for both scanning systems was connected to a data acquisition system manufactured by National Instruments (National Instruments Documentation). The data was then stored for future processing. The standard sample used for experimental measurements is shown in Fig. 13. This plate was manufactured by Olympus NDT (Olympus NDT, Documentation), and it has been chosen because of the artificial cracks have different sizes, shapes, and orientation with respect to the scanning direction.

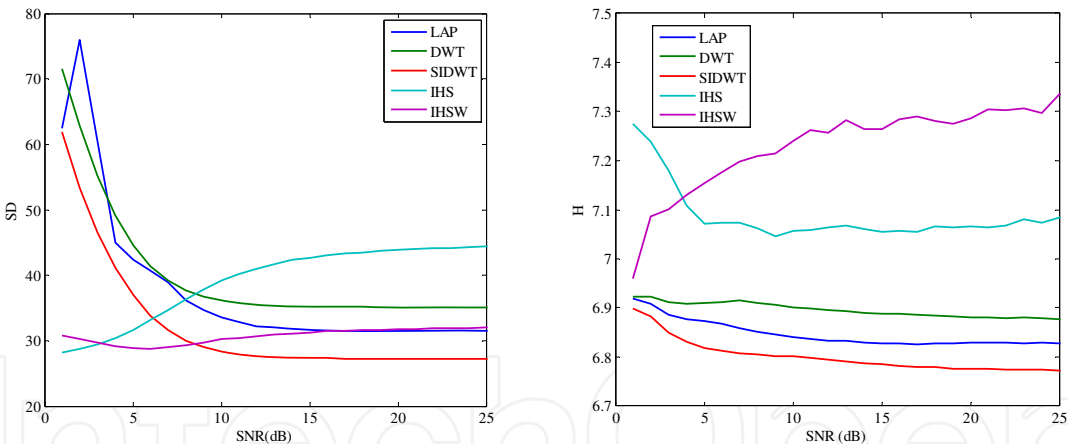


Fig. 11. Performance of fusion with standard deviation and entropy quality metric

Four experimental images at frequencies 10 kHz, 100 kHz, 300 kHz, and 800 kHz, respectively are shown in Fig. 14. These images represent the amplitude of the vertical component after the rotation of the axes to reduce the effect of liftoff noise. After the registration of EC to the optical image, three of the EC images of Fig. 14 and the optical image were used as input to the fusion algorithms. IHS and IHSW use three EC images as input to the IHS transform, and optical image as the HR image, while the other fusion methods LAP, DWT, and SIDWT normally accept two input images only, so a multi-stage fusion process were conducted for the comparison. A comparison using the three lowest frequency value images and the three highest frequency images of Fig. 12 are shown in Fig. 15 and Fig. 16 respectively. Notice that with high frequency images used, the good resolution of the fused images is noticeable.

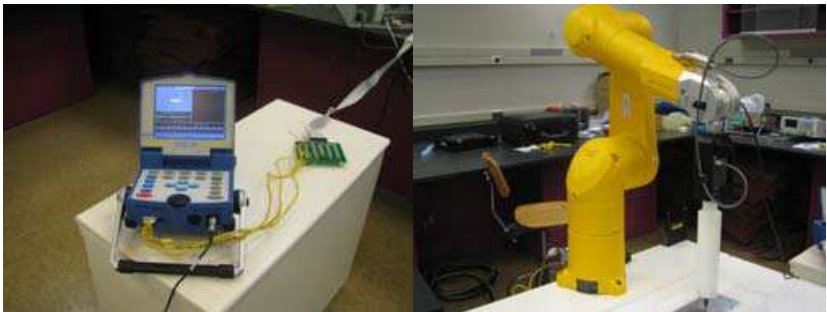


Fig. 12. Eddy current measurement system (Rohmann B 300) (left) and Staubli robot (right), which are the main parts of the scanning system



Fig. 13. Optical photo of the plate used in experimental measurements

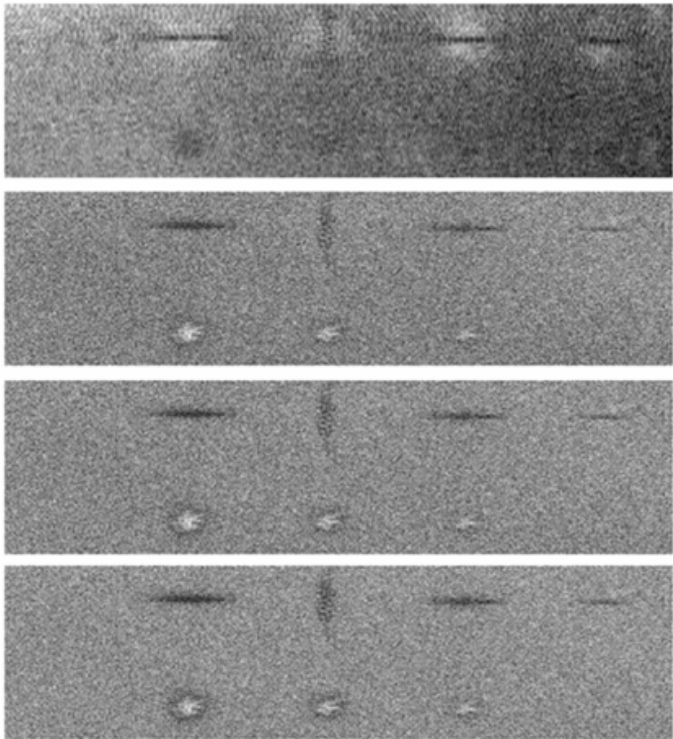


Fig. 14. Measured EC images at 10 kHz, 100 kHz, 300 kHz, and 800 kHz, top to bottom, respectively

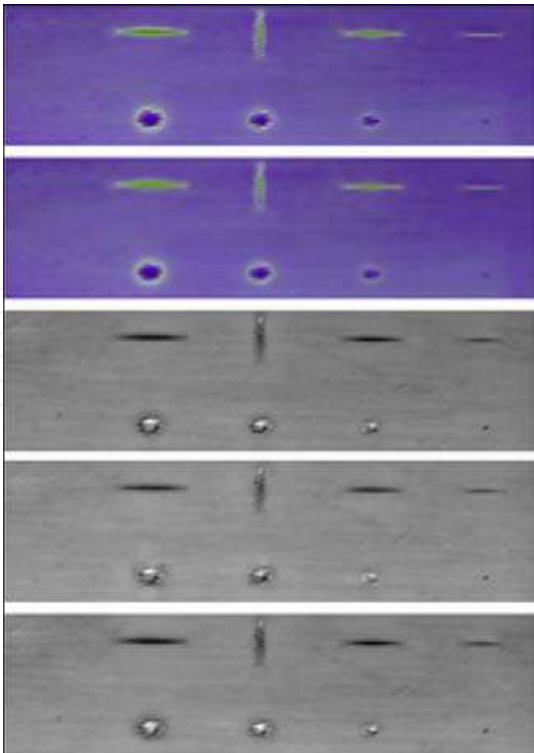


Fig. 15. Fusion results with the first three lowest frequency value images shown in Fig. 14, along with the optical image. Results reveal IHS, IHSW, SIDWT, DWT, LAP fusion, top to bottom, respectively

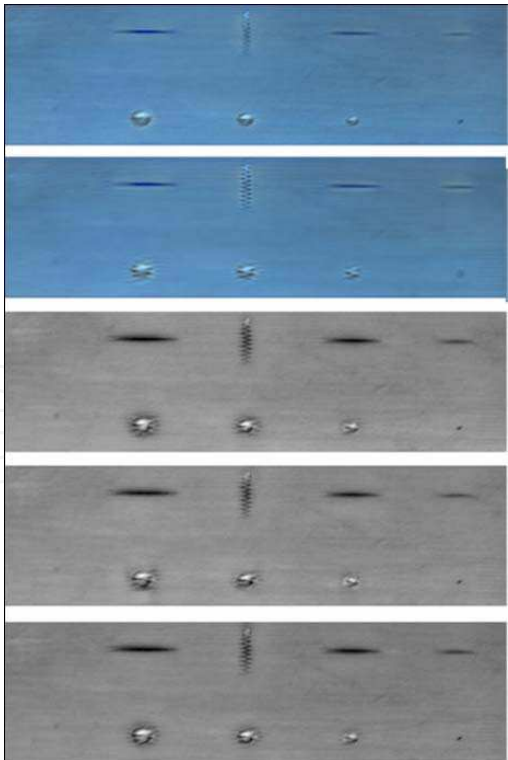


Fig. 16. Fusion results with the last three highest frequency value images shown in Fig. 14, along with the optical image. Results reveal IHS, IHSW, SIDWT, DWT, LAP fusion, top to bottom, respectively

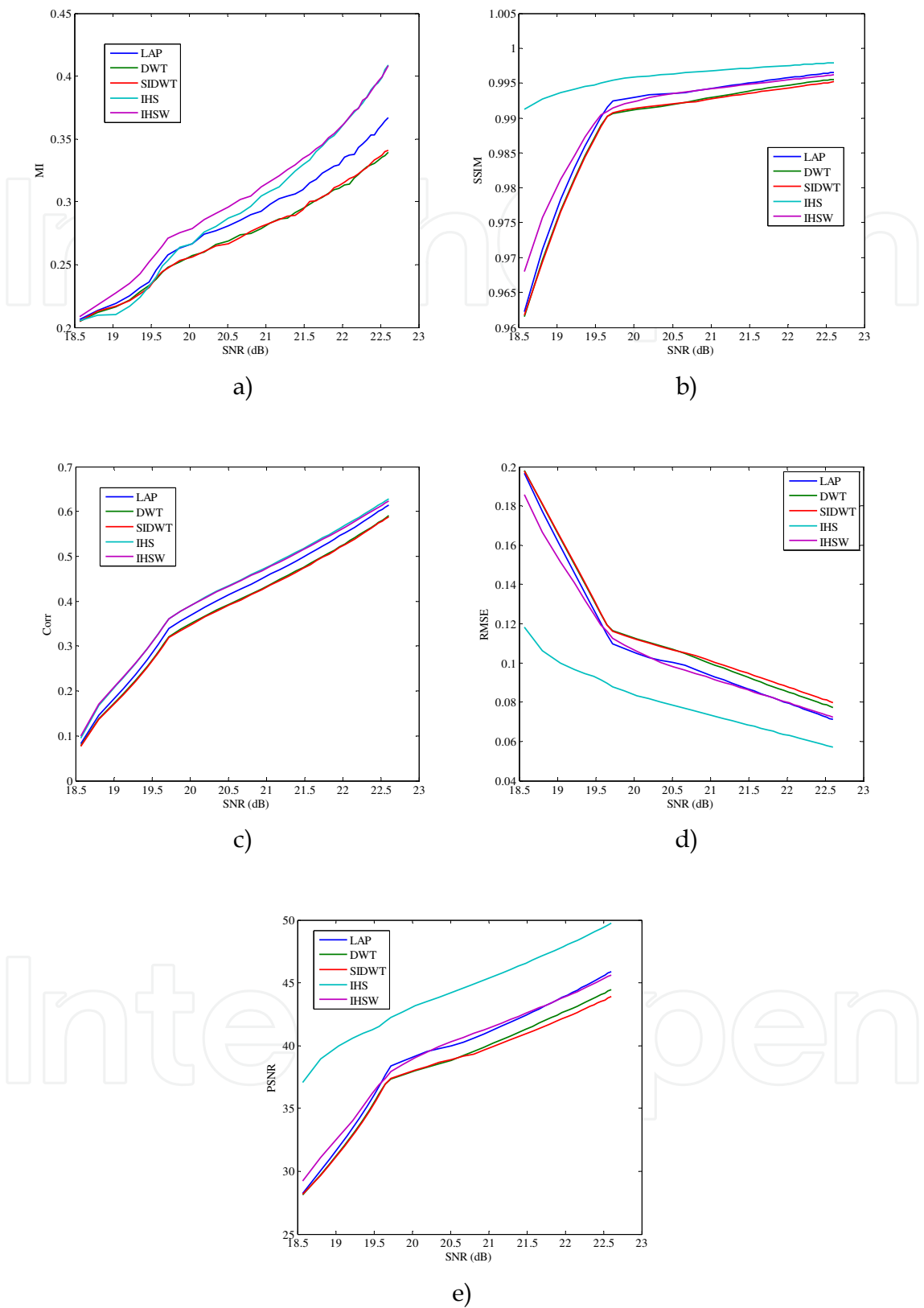


Fig. 17. Performance of fusion with mutual information metric (a), structure information, structural similarity metric (b), correlation metric (c), root mean square error metric (d), and peak SNR quality metric (e)

Gaussian noise added to the experimental images used as inputs to the fusion methods according to a predefined signal to noise ratio SNR, and the performance of the fusion methods were compared with five objective evaluation measures that require reference image, namely, mutual information (MI), structure information, structural similarity (SSIM), correlation coefficient (Corr), root mean square error (RMSE), and peak signal to noise ratio (PSNR). The reference image was produced depending on the standard sample used. Fig. 17 shows the results of the five mentioned metrics and how these metrics are affected by noise. Results illustrate that the IHS based methods perform better than the others three fusion methods for all performance measures used in the range of acceptable image SNR.

## 9. Conclusions and future work

The emerging concept of data fusion, particularly in NDE image fusion is used to develop robust NDE systems, which can easily be adapted in industrial applications. Novel systems are introduced implementing image fusion in electromagnetic NDE applications. The focus is directed toward the emerging techniques based on eddy current (EC) inspection methods, which are among the most promising electromagnetic inspection modalities, due to their simplicity, versatility, high sensitivity, and high speeds of testing. Results are presented for fusing conventional as well as pulsed eddy current images. EC scanning of sample under test is done based on automatic robotic system to obtain c-scan images.

Image fusion algorithms exploit both the redundancy and complementary information to enhance the robustness of the resulting image. Redundant information is used to improve the SNR and complementary information is used to augment the overall information content, which increases the accuracy and reliability of inspection systems. The developed systems can be used to fuse multi-spectral, multi-temporal, and multi-spatial information in EC images. Results reveal that the proposed fusion system performs better than conventional fusion system applied to NDE, according to the performance quality measures. Various image metrics are used to assess the quality of resulting fusion images. Effective quality metrics help automate NDE fusion systems in industrial environments. The obtained results of the objective evaluation metrics are found to be almost consistent with the subjective evaluation.

## 10. Acknowledgments

This research is funded by King Abdulaziz City for Science and Technology (KACST), Research Grant: 122-28.

## 11. References

- Algarni, A., Elshafiey, I., & Alkanhal, M. A. (2009). Multimodal Image Fusion for Next Generation NDE Systems. *IEEE International Symposium on Signal Processing and Information Technology*, (pp. 219-224).
- Ansari, F. (1992). Real Time Condition Monitoring of Concrete Structures by Embedded Optical Fibers Sensors. *Nondestructive Testing of Concrete Elements and Structures proceedings of sessions sponsored by the Engineering Mechanics Division of the American Society of Civil Engineers*.

- Blum, R. S., & Liu, Z. (2006). Multi-sensor image fusion and its applications. Boca Raton: CRC Press, Taylor & Francis Group.
- Brassard, M., Chehbaz, A., Pelletier, A., & Forsyth, D. S. (2000). Combined NDT inspection techniques for corrosion detection of aircraft structures. *Proc. 15th World Conf. Nondestructive Testing*. Rome, Italy.
- Cantor, T. R. (1984). Review of Penetrating Radar as Applied to Nondestructive Evaluation of Concrete. In V. M. Malhotra (Ed.). In *Situ/Nondestructive Testing of Concrete*. Detroit: American Concrete Institute.
- Chady, T., Sikora, R., Psuj, G., Enokizono, M., & Todaka, T. (2005). Fusion of electromagnetic inspection methods for evaluation of stress-loaded steel samples. *IEEE Trans. Magn.*, 41 (10), pp. 3721-3723.
- Chalastaras, A., Malkinski, L., Jung, J.-S., Oh, S.-L., Lee, J.-K., Ventrice, C. J., et al. (2004). GMR Multilayers on a New Embossed Surface. *IEEE Trans. Magn.*, 40, pp. 2257 - 2259.
- Chen, Y., & Blum, R. S. (2005). Experimental Tests of Image Fusion for Night Vision. *8th International Conference on Information Fusion*, ECE Dept., Lehigh Univ.
- Djafari, A. M. (July, 2002). Fusion of X-ray and geometrical data in computed tomography for nondestructive testing applications. *Proceedings of the Fifth Int. Conf. Inf. Fusion*, pp. 309-316.
- Elshafiey, I., Alkanhal, M., & Algarni, A. (2008). Image Fusion Based Enhancement of Eddy Current Nondestructive Evaluation. *International Journal of Applied Electromagnetics and Mechanics (IJAEM)*, 28 (1-2), pp. 291-296.
- Fowler, J. E. (2005). The Redundant Discrete Wavelet Transform and Additive Noise. *IEEE Signal Processing Letters*, 12, pp. 629-632.
- Francois, V., & Kaftandjian, N. (2003). Use of data fusion methods to improve reliability of inspection: Synthesis of the work done in the frame of a European thematic network. *Journal of Nondestructive Testing*, 8, pp. 1-8.
- Gonzalez, R., & Woods, R. (2007). Digital Image Processing. (3rd, Ed.) Prentice Hall.
- Gonzalez-Audicana, M., Otazu, X., Fors, O., & Alvarez-Mozos, J. (2006). A Low Computational-Cost Method to Fuse IKONOS Images Using the Spectral Response Function of Its Sensors. *IEEE Trans. Geosci. Remote Sens.*, 44, pp. 1683-1691.
- Gros, X. E., & Takahashi, K. (1998). Fusion of NDT Data Improve Inspection of Composite Materials. *Proceedings of 1998 Japanese Society of Nondestructive Inspection Spring Conference*, (pp. 265-268).
- Gros, X. E., Strachan, P., & Lowden, D. W. (1995). Theory and Implementation of NDT Data Fusion. *Res. Nondestruct. Eval.*, 6 (4), pp. 227-236.
- Gros, X., Liu, Z., Tsukada, K., & Hanasaki, K. (2000). Experimenting with Pixel-level NDT Data Fusion Techniques. *IEEE Trans. Instrumentation and Measurement*, 49, pp. 1083 - 1090.
- Jaarinen, J., Hartikainen, J., & Luukkala, M. (1989). Quantitative Thermal Wave Characterization of Coating Adhesion Defects. In *Review of Progress in Quantitative NDE*. D. O. Thompson, & D. Chimenti (Eds.): Plenum Press.
- Kaftandjian, V., Zhu, Y. M., Dupuis, O., & Babot, D. (2005). The Combined Use of the Evidence Theory and Fuzzy Logic for Improving Multimodal Nondestructive Testing Systems. *IEEE Trans. Instrumentation and Measurement*, 54 (5), pp. 1968-1977.

- Kwarteng, P. S., & Chavez, A. Y. (1989). Extracting spectral contrast in Landsat Thematic Mapper image data using selective principal component analysis. *Photogramm. Eng. Remote Sens.* , 55, pp. 339-348.
- Lee, S. J., & Song, S. H. (2005). Magneto-optic Sensor for Remote Evaluation of Surfaces. *IEEE Trans. Magn.* , 41, pp. 2257-2259.
- Li, S., et al. (2002). Using the discrete wavelet frame transform to Merge Landsat TM and SPOT Panchromatic Images. *Information Fusion* , 3, pp. 17-23.
- Liu, Z., Abbas, F., & Nezh, M. (2006). Application of Dempster-Shafer Theory for Fusion of Lap Joints Inspection Data. *Proceedings of SPIE, the International Society for Optical Engineering* , 6176.
- Liu, Z., Gros, X. E., Tsukada, K., Hanasaki, K., & Takahashi, K. (1999). The use of wavelets for pixel level NDT data fusion. *Proc. 2nd Jpn.-US Symp. Advances NDT*, (pp. 474-477). Kahuku, HI.
- Liu, Z., Tsukada, K., Hanasaki, K., & Kurisu, M. (1999). Two-Dimensional Eddy Current Signal Enhancement via Multifrequency Data Fusion. *Res. Nondestruct. Eval.* , 11 (3), pp. 165-177.
- Lord, W. (1983). Application of Numerical Field Modeling to Electromagnetic Methods of nondestructive Testing. *IEEE Trans. on Magnetics* , 19, pp. 2437-2442.
- Matuszewski, B. J., Shark, L. K., & Varley, M. R. (Oct., 2000). Region-based wavelet fusion of ultrasonic, radiographic and shearographic nondestructive testing images. *Proceedings of the 15<sup>th</sup> World Conf. Nondestructive Testing*. Rome, Italy.
- Mina, M., Udpa, S. S., Udpa, L., & Yim, J. (1997). A new approach for practical two dimensional data fusion utilizing a single eddy current probe. *Review of Progress in QNDE*, 16, pp. 749-755.
- Mina, M., Yim, J., Udpa, S. S., & Udpa, L. (1996). Two dimensional multi-frequency eddy current data fusion, (pp. 2125-2132).
- Naidu, V. P., & Raol, J. R. (2008). Pixel-level Image Fusion using Wavelets and Principal Component Analysis. *Defence Science Journal* , 58, pp. 338-352.
- National Instruments Documentation. Retrieved from [www.ni.com/dataacquisition](http://www.ni.com/dataacquisition).
- Nunez, J. O. (1999). Multiresolution based image fusion with additive wavelet decomposition. *IEEE Trans. Geosci. Remote Sens.* , 37 (3), pp. 1204 - 1211.
- Olympus NDT, Documentation. Retrieved from [www.OlympusNDT.com](http://www.OlympusNDT.com)
- Petrovic, C. X. (2000). Objective pixel level image fusion performance measure. *Proc. SPIE*, 4051, pp. 88-99. Orlando, FL.
- Rohmann Documentation. Retrieved from [www.rohmann.de](http://www.rohmann.de).
- Simone, G., & Morabito, F. C. (2001). NDT image fusion using eddy current and ultrasonic data. *Int. J. Comput. Math. Elect. Electron. Eng.* , 20 (3), pp. 857-868.
- Song, Y. W., & Udpa, S. S. (1996). A New Morphological Algorithm for Fusing Ultrasonic and Eddy Current Images. *Proc. IEEE Ultrason. Symp.*, (pp. 649-652).
- Staubli Documentation. Retrieved from [www.staubli.com/en/robotics](http://www.staubli.com/en/robotics)
- Tai, C.-C., & Pan, Y.-L. (2008). A Novel Multiphysics Sensing Method Based on Thermal and EC Techniques and its Application for Crack Inspection. *Proceedings of the 2008 IEEE International Conference on Sensor Network, Ubiquitous, and Trustworthy Computing* , pp. 475-479.
- Tania, S. (2008). Image Fusion: Algorithms and applications. London: Academic Press.

- Tian, G. Y., Sophian, A., Taylor, D., & Rudlin, J. (2005). Multiple sensors on pulsed eddy-current detection for 3-D subsurface crack assessment. *IEEE Sensors Journal* , 5, pp. 90-96.
- Toet, A. (1992). Multiscale Contrast Enhancement with Application to Image Fusion. *Optical Engineering* , 31 (5), pp. 1026-1031.
- Udpa, L. (2001). Neural Networks for NDE. Proc. IV Int. Workshop: Advances Signal Process. *Nondestructive Eval. Mater.* Quebec City, QC, Canada.
- Udpa, L., & Elshafiey, I. (2001). WINSAS: A New tool for Enhancing the Performance of Eddy Current Inspection of Aging Aircraft Wheels. Hyatt-Orlando, Orlando, Florida.
- Volponi, A. J., Brotherton, T., Luppold, R., & Simon, D. L. (2004). Development of an Information Fusion System for Engine Diagnostics and Health Management. NASA.
- Wang, Z., Bovik, A. C., Sheikh, H. R., & Simoncelli, E. P. (2004). Image Quality Assessment: From Error Visibility to Structural Similarity. *IEEE Transactions on Image Processing* , 13, pp. 600 - 612.
- Wang, Z., Ziou, D., Armenakis, C., Li, D., & Li, Q. (2005). A Comparative Analysis of Image Fusion Methods. *IEEE Transactions on Geoscience and Remote Sensing* , 43, pp. 1391-1402.
- Yim, J. (1995). Image Fusion Using Multiresolution Decomposition and LMMSE Filter. Ph.D. dissertation, Iowa State Univ.
- Yim, J., Udpa, S. S., Mina, M., & Udpa, L. (1996). Optimum Filter Based Techniques for Data Fusion. *Review of Progress in Quantitative NDE*. D. O. Thompson, & D. Chimenti (Eds.): Plenum Press. pp. 773-780.
- Yim, J., Udpa, S. S., Udpa, L., & Lord, W. (1995). Neural Network Approaches to Data Fusion. In D. O. Thompson, & D. E. Chimenti (Ed.), *Review of Progress in QNDE*. 14, pp. 819-826. New York: Plenum.
- Zitova, B., & Flusser, J. (2003). Image registration methods: a survey. *Image and Vision Computing* , 21, pp. 977-1000.

IntechOpen

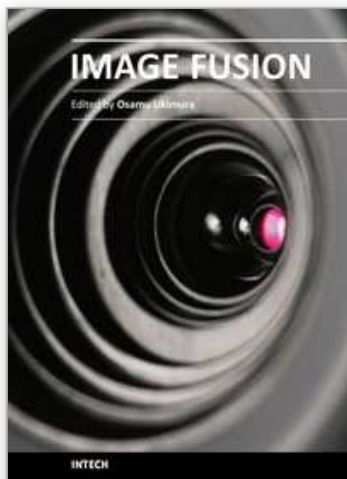


## **Image Fusion**

Edited by Osamu Ukimura

ISBN 978-953-307-679-9

Hard cover, 428 pages

**Publisher** InTech

**Published online** 12, January, 2011

**Published in print edition** January, 2011

Image fusion technology has successfully contributed to various fields such as medical diagnosis and navigation, surveillance systems, remote sensing, digital cameras, military applications, computer vision, etc. Image fusion aims to generate a fused single image which contains more precise reliable visualization of the objects than any source image of them. This book presents various recent advances in research and development in the field of image fusion. It has been created through the diligence and creativity of some of the most accomplished experts in various fields.

### **How to reference**

In order to correctly reference this scholarly work, feel free to copy and paste the following:

Ibrahim Elshafiey, Ayed Algarni and Majeed A. Alkanhal (2011). Image Fusion Based Enhancement of Nondestructive Evaluation Systems, Image Fusion, Osamu Ukimura (Ed.), ISBN: 978-953-307-679-9, InTech, Available from: <http://www.intechopen.com/books/image-fusion/image-fusion-based-enhancement-of-nondestructive-evaluation-systems>

**INTech**  
open science | open minds

### **InTech Europe**

University Campus STeP Ri  
Slavka Krautzeka 83/A  
51000 Rijeka, Croatia  
Phone: +385 (51) 770 447  
Fax: +385 (51) 686 166  
[www.intechopen.com](http://www.intechopen.com)

### **InTech China**

Unit 405, Office Block, Hotel Equatorial Shanghai  
No.65, Yan An Road (West), Shanghai, 200040, China  
中国上海市延安西路65号上海国际贵都大饭店办公楼405单元  
Phone: +86-21-62489820  
Fax: +86-21-62489821

© 2011 The Author(s). Licensee IntechOpen. This chapter is distributed under the terms of the [Creative Commons Attribution-NonCommercial-ShareAlike-3.0 License](https://creativecommons.org/licenses/by-nc-sa/3.0/), which permits use, distribution and reproduction for non-commercial purposes, provided the original is properly cited and derivative works building on this content are distributed under the same license.

IntechOpen

IntechOpen